Reduction of Acute Inflammatory Effects of Fumed Silica Nanoparticles in the Lung by Adjusting Silanol Display through Calcination and Metal Doping

Bingbing Sun,[†] Suman Pokhrel,[‡] Darren R. Dunphy,[§] Haiyuan Zhang,[∥] Zhaoxia Ji,[⊥] Xiang Wang,[⊥] Meiying Wang,[†] Yu-Pei Liao,[†] Chong Hyun Chang,[⊥] Juyao Dong,[#] Ruibin Li,[†] Lutz Mädler,[‡] C. Jeffrey Brinker,[§,¶,▲] André E. Nel,[*,†,⊥] and Tian Xia[*,†,⊥]

[†]Division of NanoMedicine, Department of Medicine, [⊥]California NanoSystems Institute, and [#]Department of Chemistry, University of California, Los Angeles, California 90095, United States, [‡]Foundation Institute of Materials Science (IWT), Department of Production Engineering, University of Bremen, 28359 Bremen, Germany, [§]Department of Chemical and Nuclear Engineering and [¶]Department of Molecular Genetics and Microbiology, University of New Mexico, Albuquerque, New Mexico 87131, United States, [∥]Laboratory of Chemical Biology, Changchun Institute of Applied Chemistry, Chinese Academy of Sciences, Changchun 130022, Jilin, China, and [▲]Self-Assembled Materials Department, Sandia National Laboratories, P.O. Box 5800 MS1349, Albuquerque, New Mexico 87185, United States

ABSTRACT The production of pyrogenic (fumed) silica is increasing worldwide at a 7% annual growth rate, including expanded use in food, pharmaceuticals, and other industrial products. Synthetic amorphous silica, including fumed silica, has been generally recognized as safe for use in food products by the Food and Drug Administration. However, emerging evidence from experimental studies now suggests that fumed silica could be hazardous due to its siloxane ring structure, high silanol density, and "string-of-pearl-like" aggregate structure, which could combine to cause membrane disruption, generation of reactive oxygen species, pro-inflammatory effects, and liver fibrosis. Based on this structure—activity analysis (SAA), we investigated whether calcination and rehydration of fumed silica changes its hazard potential in the lung due to an effect on silanol density display. This analysis demonstrated that the accompanying change in surface reactivity could indeed impact cytokine production in macrophages and acute inflammation in the lung, in a manner that is dependent on siloxane ring reconstruction. Confirmation of this SAA *in vivo*, prompted us to consider safer design of fumed silica properties by titanium and aluminum doping (0—7%), using flame spray pyrolysis. Detailed characterization revealed that increased Ti and Al doping could reduce surface silanol density and expression of three-membered siloxane rings, leading to dose-dependent reduction in hydroxyl radical generation, membrane perturbation, potassium efflux, NLRP3 inflammasome activation, and cytotoxicity in THP-1 cells. The reduction of NLRP3 inflammasome activation was also confirmed in bone-marrow-derived macrophages. Ti doping, and to a lesser extent Al doping, also ameliorated acute pulmonary inflammation, demonstrating the possibility of a safer design approach for fumed silica, should that be required for specific use circumstances.

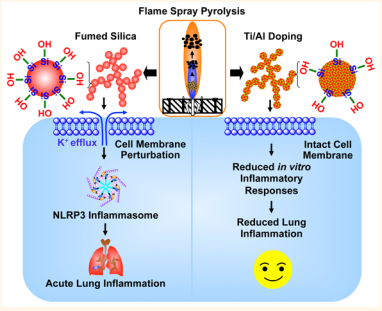

KEYWORDS: fumed silica · silanol groups · doping · NLRP3 inflammasome · IL-1β · lung inflammation

Fumed silica consumption worldwide has been projected to continue to grow at a rate of 7% annually, reaching a production volume of 1.7 million metric tons in 2018 for applications such as food, pharmaceuticals, electronics, rubber, plastics, paints, desiccants, and cosmetics.[1] As a form of synthetic amorphous silica (SAS), fumed silica is generally recognized as safe (GRAS) for food additives and food packaging by the Food and Drug Administration (FDA).[2,3] SAS, including fumed silica, has been regarded as a safe material for decades with no environmental or health risks being reported for these materials. However, recent experimental evidence has been obtained showing that fumed silica, different from colloidal and Stöber silica, could generate cytotoxicity and pro-inflammatory effects *in vitro* and *in vivo*.[4−6] Cellular studies have revealed that fumed silica could cause dose- and time-dependent cytotoxicity,[7] DNA damage, glutathione depletion,[8] red blood cell lysis, and pro-inflammatory effects, including NLRP3 inflammasome activation.[4,5] Moreover, rodent inhalation studies showed that fumed silica could induce injurious and pro-inflammatory effects in the lung (*e.g.*, increases in neutrophils,

* Address correspondence to txia@ucla.edu, anel@mednet.ucla.edu.

Received for review June 6, 2015 and accepted July 22, 2015.

Published online July 22, 2015
10.1021/acsnano.5b03443

albumin, alkaline phosphatase, and lactate dehydrogenase in bronchoalveolar lavage fluid), although these effects were partially reversible.[6] In addition, when fumed silica was delivered orally, it was found to accumulate in the spleen and (at high dosages) the liver, causing formation of granulomas.[9] In a recent communication, Maynard called out the apparent discrepancy between the widely accepted safety profile of fumed silica being used in consumer products *versus* the experimental demonstration of hazard,[3] which even exceeds that of quartz.[5] Against this background, we set out to explore the possibility of whether the *in vitro* injurious effects could be duplicated in the lung, and whether it is possible to provide a safer designed version of fumed silica should that be necessitated by use circumstances that could lead to hazard.

It is possible through the use of adverse outcome pathway analysis to establish structure−activity relationships (SARs) that can be used for the safer design of engineered nanomaterials (ENMs).[10,11] Recently, Zhang *et al.* demonstrated that the membrane lytic potential and cytotoxicity of fumed silica could be attributed to specific surface properties as a result of the reconstruction of strained three-membered rings (3MRs) and surface display of silanols groups.[5] The density of surface silanol groups (≡Si−OH), which are partially deprotonated at physiological pH to form ≡Si−O$^-$, determines the magnitude of electrostatic interaction between the fumed silica surface and membrane phospholipids.[5,12,13] This could lead to disruption of plasma membrane integrity, resulting in hemolysis of red blood cells.[5,14,15] Another SAR related to the cleavage of strained 3MRs at the particle surface is the generation of hydroxyl radicals, which could further enhance plasma membrane perturbation and the generation of a danger signal that leads to the assembly of the NLRP3 inflammasome (Scheme 1).[5,16,17] The inclusion of caspase-1 in this activated inflammasome complex allows cleavage of pro-interleukin-1β (pro-IL-1β) and IL-1β release from macrophages; this cytokine plays a major role in pulmonary inflammation by a variety of ENMs.[18,19] Based on these findings, we hypothesized that pro-inflammatory effects at cellular and pulmonary levels could be used as an adverse outcome pathway to investigate the potential for safer design of fumed silica through a reduction of the number of 3MRs as well as of surface density display of silanols.

A number of approaches are available to modify the surface reactivity of engineered nanomaterials, including calcination,[5,20] doping,[21−23] surface coating,[18,24] and modification of surface charge.[25−27] We chose calcination and doping because these are comparatively simple and effective methods for modifying the surface of nanomaterials. While calcination could reduce the surface silanol content *via* condensation (*e.g.*, ≡Si−OH + HO-Si≡ ⇔ ≡Si−O−Si≡ + H_2O), the reverse reaction as a result of the hydrolysis of siloxane bonds can regenerate these silanols.[5] Thus, the reduced silanol concentration resulting from calcination is not permanent and is subject to change by the humidity of the surrounding environment, including immersion in water or aqueous biological fluids. On the other hand, doping by flame spray pyrolysis (FSP) offers a one-step approach for the synthesis of homogeneous and high-purity nanomaterials.[28] In this context, a previous study has shown that aluminum (Al) doping of the silica framework could decrease its surface reactivity by reducing the surface concentration of the hydrogen-bonded vicinal silanol groups.[29,30] In addition to Al, titanium (Ti) was considered as a dopant due to its high biocompatibility of its oxide forms.[31,32] Using calcined and rehydrated as well as doped fumed silica, we assembled a library of fumed silica nanoparticles to study the relationship of surface silanol display and 3MR to pro-inflammatory responses in macrophages and the murine lung. In brief, we observed that a reduction in reactive surface silanol display is effective at reducing acute pulmonary inflammation and pro-inflammatory effects in macrophages. Thus, we have developed a blueprint for reducing the toxicity of fumed silica for user applications where inhalation and possibly other exposures could constitute a hazard that may not otherwise be considered given that fumed silica is GRAS.

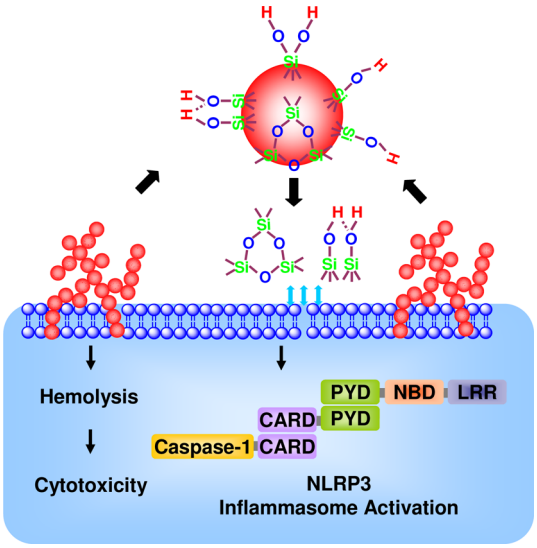

Scheme 1. Structure−activity relationship showing the cleavage of strained 3MRs at the particle surface causes the generation of hydroxyl radicals, which could further enhance plasma membrane perturbation and the generation of a danger signal that leads to the assembly of the NLRP3 inflammasome.

RESULTS

Acute Pro-inflammatory Effects of Fumed Silica in the Lung Is Attenuated by Calcination but Exacerbated by Rehydration. We have previously demonstrated that fumed silica is capable of inducing hemolysis and cytotoxicity, which could be decreased by reducing the surface hydroxyl content and the population of surface 3MRs through

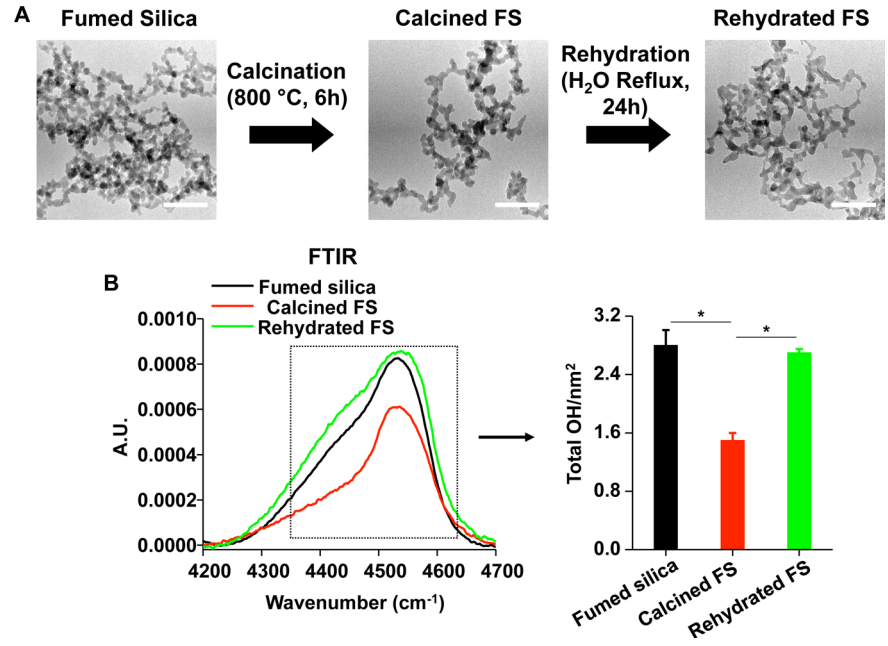

Figure 1. Physicochemical characterization of calcined and rehydrated fumed silica nanoparticles. (A) Representative TEM images of fumed silica nanoparticles. The images were taken with a JEOL 1200 EX TEM with an accelerating voltage of 80 kV. The scale bar is 50 nm. (B) Fourier transform infrared (FTIR) analysis of the silanol concentration in fumed silica, using vibrational bands at 4500 cm^{-1}. Silanol concentration calculated through the integration of the FTIR band data at 4500 cm^{-1}; *$p < 0.05$ compared to calcined fumed silica.

TABLE 1. Hydrodynamic Size and ζ-Potential of Fumed Silica, Calcined Fumed Silica, and Rehydrated Fumed Silica

	hydrodynamic size (nm)			ζ-potential (mV)		
	water	PBS, 0.6 mg/mL BSA, and 0.01 mg/mL DPPC	RPMI 1640 and 10% serum	water	PBS, 0.6 mg/mL BSA, and 0.01 mg/mL DPPC	RPMI 1640 and 10% serum
fumed silica	229.0 ± 5.9	262.4 ± 6.4	195.2 ± 8.1	−37.0 ± 1.3	−10.5 ± 1.4	−6.7 ± 0.5
calcined fumed silica	232.3 ± 5.71	290.1 ± 11.3	235.2 ± 8.0[a]	−12.4 ± 1.7[b]	−3.7 ± 18.2	−3.4 ± 13.8
rehydrated fumed silica	236.7 ± 17.7	267.3 ± 14.9	193.9 ± 10.6	−35.6 ± 1.6	−15.5 ± 3.2	−7.1 ± 0.7

[a] $p < 0.05$ compared to the size of nondoped fumed silica in RPMI 1640 and 10% serum. [b] $p < 0.05$ compared to the ζ-potential of nondoped fumed silica in water.

calcination.[5] Moreover, rehydration of the calcined fumed silica nanoparticles could restore the hydroxyl content and toxic potential.[5] In order to see if this SAR also applies to the intact lung, we prepared a batch of calcined silica particles by heating at 800 °C for 6 h as well as rehydrating the heated particles by water reflux for 24 h, as previously described[5] (Figure 1). Calcination and rehydration did not change the primary particle size; however, calcination marginally, but significantly, changed the aggregation state and ζ-potential of fumed silica in RPMI 1640 (plus 10% serum) and water, respectively (Figure 1A and Table 1).

Following oropharyngeal aspiration of 40 μg particles per mouse ($n = 6$ animals/group) and animal sacrifice after 40 h, we obtained clear evidence that calcined silica induced significantly less ($p < 0.05$) neutrophil infiltration than pristine fumed silica (Figure 2A). In contrast, rehydration of the calcined particles restored the acute pro-inflammatory effects. Confirmatory evidence was provided by ELISA microarrays, which were used to assess cytokine and chemokine content in the BAL fluid. This sensitive assay, performed at Pacific Northwest National Laboratory, allows high-throughput measurement of multiple cytokines contemporaneously. Fumed silica significantly increased ($p < 0.05$) macrophage inflammatory protein-1α (MIP-1α), macrophage inflammatory protein-1γ (MIP-1γ), macrophage-derived chemokine (MDC), monocyte chemoattractant protein-1 (MCP-1), IL-6, granulocyte colony-stimulating factor (G-CSF), vascular endothelial growth factor (VEGF), and thymus and activation regulated chemokine (TARC) production (Figure 2B−F and Supporting Information Figure S1). While calcination of the fumed silica reduced cytokine production, rehydration of the particles restored the pro-inflammatory effects to levels approaching that of pristine fumed silica (Figure 2B−F and Supporting Information Figure S1). Histological examination of the lungs, following hematoxylin and eosin (H&E) staining, helped to confirm (Figure 2G) that pristine and rehydrated fumed silica could induce acute inflammatory changes that correlate with high surface

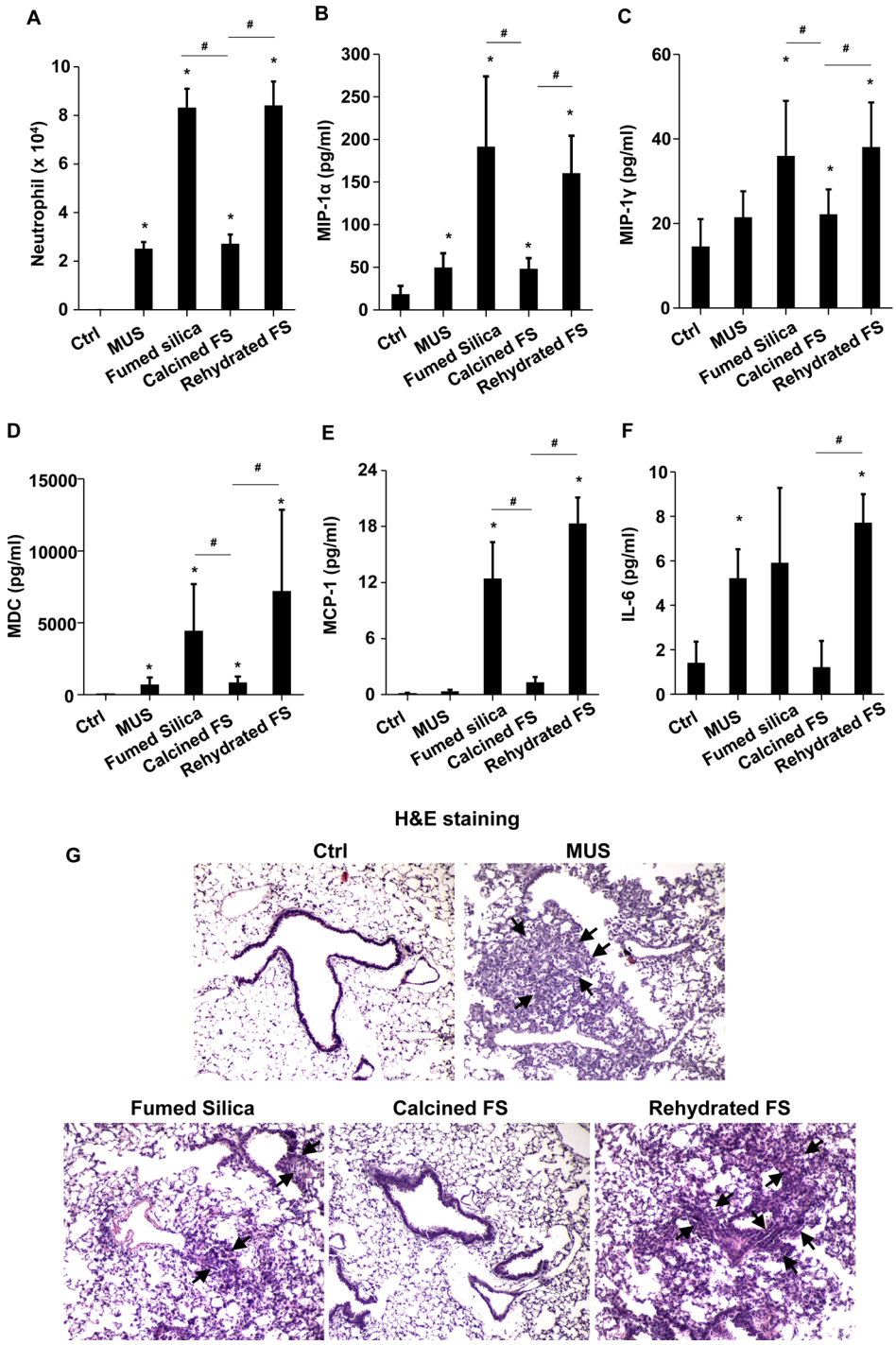

Figure 2. Acute pro-inflammatory effects of fumed silica in the lung is attenuated by calcination but exacerbated by rehydration. C57BL/6 ($n = 6$) mice were exposed to 1.6 mg/kg of pristine, calcined, and rehydrated fumed silica nanoparticles by oropharyngeal aspiration for 40 h, then animals were sacrificed to collect BAL fluid and lung tissue. (A) Neutrophil count; *$p < 0.05$ compared to control mice; #$p < 0.05$ compared to calcined fumed-silica-treated mice. An ELISA microarray assay was used to measure the following cytokine and chemokine levels including (B) MIP-1α, (C) MIP-1γ, (D) MDC, (E) MCP-1, and (F) IL-6. MIN-U-SIL, a natural form of crystalline silica, was used as a positive control; *$p < 0.05$ compared to control mice; #$p < 0.05$ compared to calcined fumed-silica-treated mice. (G) H&E staining showing focal inflammation induced by fumed silica. Calcination of the particles attenuated lung inflammation but rehydrated fumed silica nanoparticles exacerbated the inflammatory effects. The regions of focal inflammation are indicated by the arrows.

silanol density, while a reduction of surface silanol density following calcination was accompanied by reduced inflammatory infiltrates in the lung. This led to the hypothesis that the synthesis of fumed silica with a decreased silanol density could be used as a safer design method.

Use of Metal Doping To Synthesize Fumed Silica Nanoparticles with Reduced Silanol Density and Surface Reactivity. Although

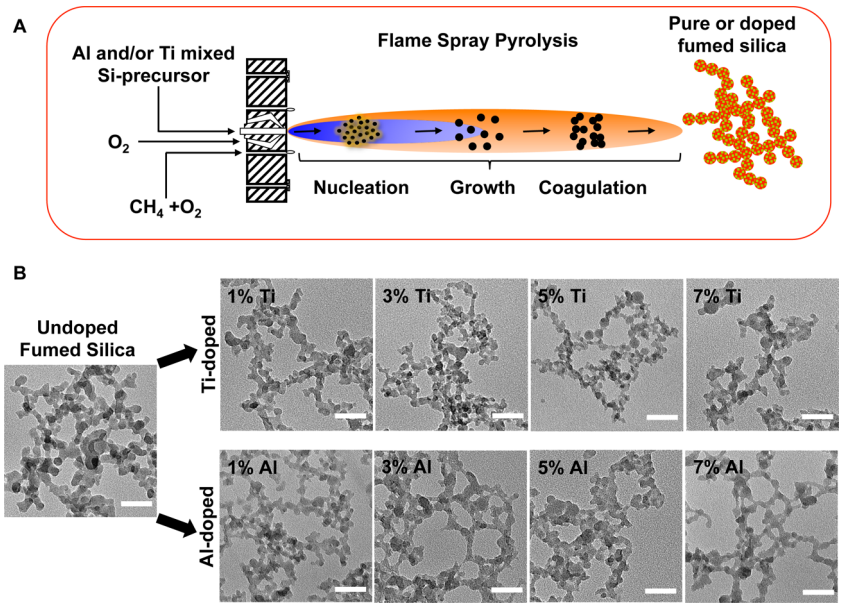

Figure 3. (A) Schematic representation of the flame spray pyrolysis process. (B) Representative TEM images of nondoped, Ti-doped, and Al-doped fumed silica nanoparticles. The images were taken with a JEOL 1200 EX TEM with an accelerating voltage of 80 kV. The scale bar is 50 nm.

calcination yields less hazardous fumed silica, this process is reversible, time-dependent, labor-intensive, and results in particles with variable surface reactivity depending on humidity fluctuations in the environment. Potentially more efficacious and simpler methods for the modulation of silanol density are available, such as doping,[21−23] surface coating,[18,24] and surface charge modification, *etc.*[25−27] We chose doping because it is a simple, one-step, and easily controllable process, and we selected Ti and Al as the dopants because of the high biocompatibility of their oxide forms.[31,32] Moreover, it has also been demonstrated that Al doping of fumed silica could decrease surface reactivity by reducing the number and density of surface hydrogen-bonded vicinal silanol groups.[29,30] Utilizing a single flame spray process, we synthesized combinatorial Ti- and Al-doped fumed silica libraries, in which the precursor, tetraethylorthosilicate (TEOS), was mixed with incremental quantities (0, 1, 3, 5, and 7 wt %) of titanium isopropoxide or aluminum secondary butoxide dopants in the mixture. Particles were formed by reaction, nucleation, surface growth, coagulation, and coalescence in the flame environment (Figure 3A). Both libraries consisted of string-of-pearl-like aggregates, as revealed by transmission electron microscopy (TEM) (Figure 3B). The primary particle size of the nondoped particles was 16 ± 2 nm. Noteworthy, incremental levels of Ti or Al doping did not significantly change primary fumed silica sizes (Figure 3 and Table 2). Also present in the Ti- and Al-doped fumed silica was a small percentage of larger, phase-separated particles (data not shown). We also determined the hydrodynamic particle sizes in the exposure media for cellular studies (RPMI 1640 plus 10% fetal calf serum) or a surrogate lung lining fluid, namely, phosphate-buffered saline (PBS), supplemented with 0.6 mg/mL of BSA (bovine serum albumin) plus 0.01 mg/mL of dipalmitoylphosphatidylcholine (DPPC) (Figure S2A−C and G and Table 2). The hydrodynamic sizes of doped and nondoped particles are in the range of 65−334 nm. In general, all fumed silica nanoparticles were better dispersed in complete cell culture media (65−191 nm) than in water (161−328 nm) or PBS supplemented with BSA and DPPC (140−334 nm). This likely reflects the dispersal effect of BSA as a result of the formation of a protein corona on the particle surface, which contributes to suspension stability[33] (Table 2). All the particles exhibited negative surface charges (−38 to −6 mV) as indicated by ζ-potential measurements in different exposure media (Table 2 and Supporting Information Figure S2D−F). Ti and Al doping produced a modest but generally insignificant reduction in the ζ-potential compared to that in nondoped fumed silica, which could be attributed to reduced hydroxyl content.

Detailed characterization was performed to confirm the incorporation of the dopants in the fumed silica matrix. First, energy-dispersive X-ray spectroscopy was used to determine the atomic percentage of each dopant in the fumed silica aggregates (Figure 4A,B and Supporting Information Figure S3A). For Ti particles, a linear relationship between Ti/Si and doping percentage was found, with small area diffraction (SAD) finding no crystalline phase within these particles, indicating homogeneous incorporation of Ti into the silica framework. X-ray diffraction (XRD) and Raman analysis (data not shown) confirmed the presence of anatase at the higher doping percentage. For Al doping, the Al/Si ratio in the fumed silica aggregates did not increase above 1% Al, suggesting phase separation of Al above this level

TABLE 2. Hydrodynamic Size and ζ-Potential of Nondoped and Doped Fumed Silica

		hydrodynamic size (nm)			ζ-potential (mV)		
	primary size (nm)	water	PBS, 0.6 mg/mL BSA, and 0.01 mg/mL DPPC	RPMI 1640 and 10% serum	water	PBS, 0.6 mg/mL BSA, and 0.01 mg/mL DPPC	RPMI 1640 and 10% serum
fumed silica	16 ± 2	258.2 ± 31.3	211.4 ± 8.6	175.3 ± 12.3	−38.0 ± 5.9	−9.5 ± 4.5	−6.8 ± 2.7
FS-1% Ti	16 ± 2	265.2 ± 11.2	266.5 ± 7.8[b]	136.0 ± 17.3[c]	−30.9 ± 2.1	−9.1 ± 7.9	−9.1 ± 2.6
FS-3% Ti	16 ± 2	182.2 ± 4.2[a]	183.3 ± 15.9	189.8 ± 10.1	−32.0 ± 3.2	−8.7 ± 5.3	−13.9 ± 8.8
FS-5% Ti	16 ± 1	300.0 ± 43.5	334.3 ± 29.9[b]	163.2 ± 6.2	−34.7 ± 7.1	−11.6 ± 3.3	−8.6 ± 4.6
FS-7% Ti	16 ± 1	247.4 ± 16.7	140.1 ± 29.8[b]	65.2 ± 16.4[c]	−34.2 ± 1.1	−15.7 ± 2.4	−10.4 ± 6.6
FS-1% Al	16 ± 1	273.2 ± 15.1	229.4 ± 8.3	117.3 ± 3.7[c]	−32.3 ± 4.9	−11.6 ± 7.0	−10.0 ± 3.2
FS-3% Al	16 ± 1	255.7 ± 7.0	293.5 ± 54.6	191.4 ± 6.9	−35.6 ± 2.8	−9.5 ± 5.0	−11.7 ± 5.8
FS-5% Al	16 ± 2	328.3 ± 26.0[a]	252.4 ± 11.6[b]	189.6 ± 10.1	−27.1 ± 4.7	−11.7 ± 6.5	−6.2 ± 4.6
FS-7% Al	16 ± 1	161.0 ± 1.3[a]	149.5 ± 7.6[b]	157.8 ± 1.0	−36.9 ± 2.7	−13.2 ± 20.3	−10.7 ± 2.1

[a] $p < 0.05$ compared to the size of nondoped fumed silica in water. [b] $p < 0.05$ compared to the size of nondoped fumed silica in PBS, 0.6 mg/mL BSA, and 0.01 mg/mL DPPC. [c] $p < 0.05$ compared to the size of nondoped fumed silica in RPMI 1640 and 10% serum.

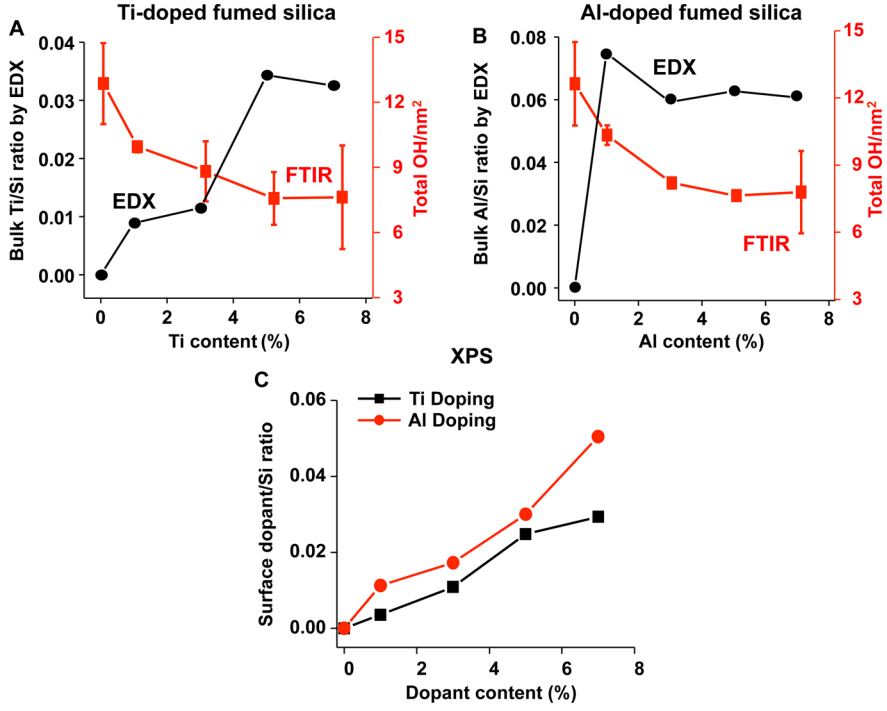

Figure 4. Physicochemical characterization of doped fumed silica nanoparticles. Energy-dispersive X-ray spectroscopy analysis shows the incremental doping of (A) Ti and (B) Al in fumed silica. The silanol concentration of (A) Ti- and (B) Al-doped fumed silica nanoparticles was calculated through the integration of the FTIR bands at 4500 cm^{-1} (total silanol). (C) X-ray photoelectron spectroscopy analysis showing the surface dopant to silica ratio of Ti- and Al-doped fumed silica nanoparticles.

during flame synthesis. However, SAD (of aggregates as well as phase-separated particles), Raman, and XRD (data not shown) failed to detect a crystalline phase in our Al-doped materials. For both Ti- and Al-doped materials, Fourier transform infrared spectroscopy (FTIR) suggested the formation of new chemical bonds between the dopants and silicon (Figure S3B–D), although overlap between the Si–OH vibrational band at 950–975 cm^{-1} (present in the nondoped fumed silica, even after calcination) and bands associated with Si–O–Ti or Si–O–Al[34,35] makes this assignment difficult (Figure S3B–D). Importantly, we believe that the presence of phase-separated material had no effect on toxicological activity, as evidenced by control studies of nondoped fumed silica mixed with TiO_2 or Al_2O_3 particles (*vide infra*). X-ray photoelectron spectroscopy was used to analyze the surface dopant/Si ratio (at a depth of several nanometers) to determine if there was dopant segregation or enrichment at the fumed silica surface. For both Ti- and Al-doped particles, we observed a monotonic increase in surface dopant concentration with incremental amounts of dopant (0–4.79 wt % Ti and 0–4.96 wt % Al) (Figure 4C), indicating lack of surface segregation or enrichment of dopants over bulk concentrations. To examine if the presence of dopants in fumed silica is indeed capable

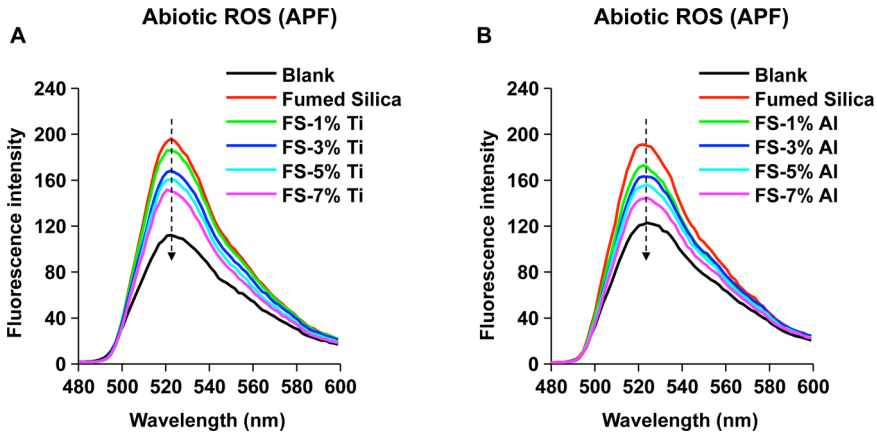

Figure 5. Abiotic ROS generation by fumed silica nanoparticles. Hydroxyl radical generation by (A) Ti- and (B) Al-doped fumed silica nanoparticles was determined by the APF. Nondoped and doped fumed silica nanoparticles (100 μg/mL) were incubated with 10 μmol/L of APF (in PBS) in a volume of 100 μL in a 96-well plate at room temperature for 6 h. Fluorescence was collected at a wavelength of 480−600 nm with an excitation wavelength at 455 nm in a microplate reader.

of changing the surface densities of silanols as well as strained 3MR, we used FTIR to determine silanol concentrations and Raman spectroscopy to determine the ring concentration.[5] To determine the total silanol content, the combination band at 4500 cm^{-1} (Figure S4A,B) was used to calculate Si−OH/nm^2.[5] The nondoped fumed silica exhibited a total silanol content of ~13 OH/nm^2 (Figure 4A,B). This number is significantly higher than that previously reported for commercial pyrolytic fumed silica.[5] However, the present material differs from the commercial product in that we utilized the combustion of hydrocarbon precursors in a CH_4/O_2 flame, whereas the commercial product is produced by pyrolysis of $SiCl_4$ in H_2/O_2. This difference in pyrolysis chemistry is reflected by a reduced siloxane condensation (*i.e.*, higher silanol content) in our material. A 1% doping of either Ti or Al results in a similar decrease in silanol concentration to between 10 and 11 OH/nm^2, with further addition leading to a more gradual reduction to about 8 OH/nm^2 above a doping level of 5%. In contrast to the total silanol content, the concentration of non-hydrogen-bonded (isolated) silanols, measured using the IR band at 3745 cm^{-1},[5] is largely invariant over the range of doping levels examined in this work (Figure S4C). Peak fitting of Raman spectra was used to determine the relative 3MR concentration by normalizing the area of the 3MR peak at ~610 cm^{-1} to the total area of the band at 800 cm^{-1}, a feature which has been assigned to silica framework vibrations.[5] We found with an increase in the Ti doping percentage from 0 to 5 wt %, there is a decrease in 3MR densities from 0.81 to 0.48 (Figure S4D). However, the measurement of the 3MR concentration in Al-doped fumed silica was complicated by the presence of autofluorescence. All considered, these results indicate that Ti or Al doping reduces the surface silanol density of the fumed silica particle surface.

Since we have shown that the silanol and 3MR concentrations of fumed silica correlate with its ability to generate reactive oxygen species (ROS),[5] we assessed ROS generation by an abiotic aminophenyl fluorescein (APF) assay, which detects hydroxyl radicals.[22] While fumed silica could induce significant hydroxyl radical generation ($p < 0.05$) (Figures 5 and S5), similar to what we previously reported,[5] incremental Ti and Al doping resulted in a progressive decline in hydroxyl radical generation (Figures 5 and S5), suggesting a reduction of their toxicological potential.

Doping Ameliorates Binding Interactions and Perturbation of the Plasma Membrane in THP-1 Cells. We have previously shown that fumed silica nanoparticle aggregates bind tightly to the surface membrane of mammalian cells, causing hemolysis of red blood cells and inducing cellular ROS production and pro-inflammatory effects.[5] In order to compare the effects of doped particles, fluorescein isothiocyanate (FITC) labeling was performed to study particle interactions with the membrane of THP-1 cells, a monocyte-derived macrophage-like cell type commonly used for cellular studies of the pro-inflammatory effects of nanomaterials.[18,36] Following cellular incubation with the green fluorescent particles, confocal microscopy demonstrated that while pristine nanoparticles were mostly localized to the cell membrane (red) without cellular uptake (Figure 6A,B) (as previously reported by us),[5] Ti- or Al-doped particles were mostly taken up by the cells, without adherence to the plasma membrane (Figure 6A,B). The use of TEM to more closely examine the interaction between fumed silica with the cell membrane demonstrated that fumed silica attaches to the plasma membrane and uses chain-like extensions to penetrate the membrane (Figure 6C). In contrast, no membrane attachment could be observed in Ti- or Al-doped nanoparticles, which were mainly taken up by membrane-bound vesicles in the cytoplasm (Figure S6).

The functional consequences of plasma membrane association by fumed silica were assessed by measuring the membrane potential through the use of a commercial dye that can be detected by a fluorometric

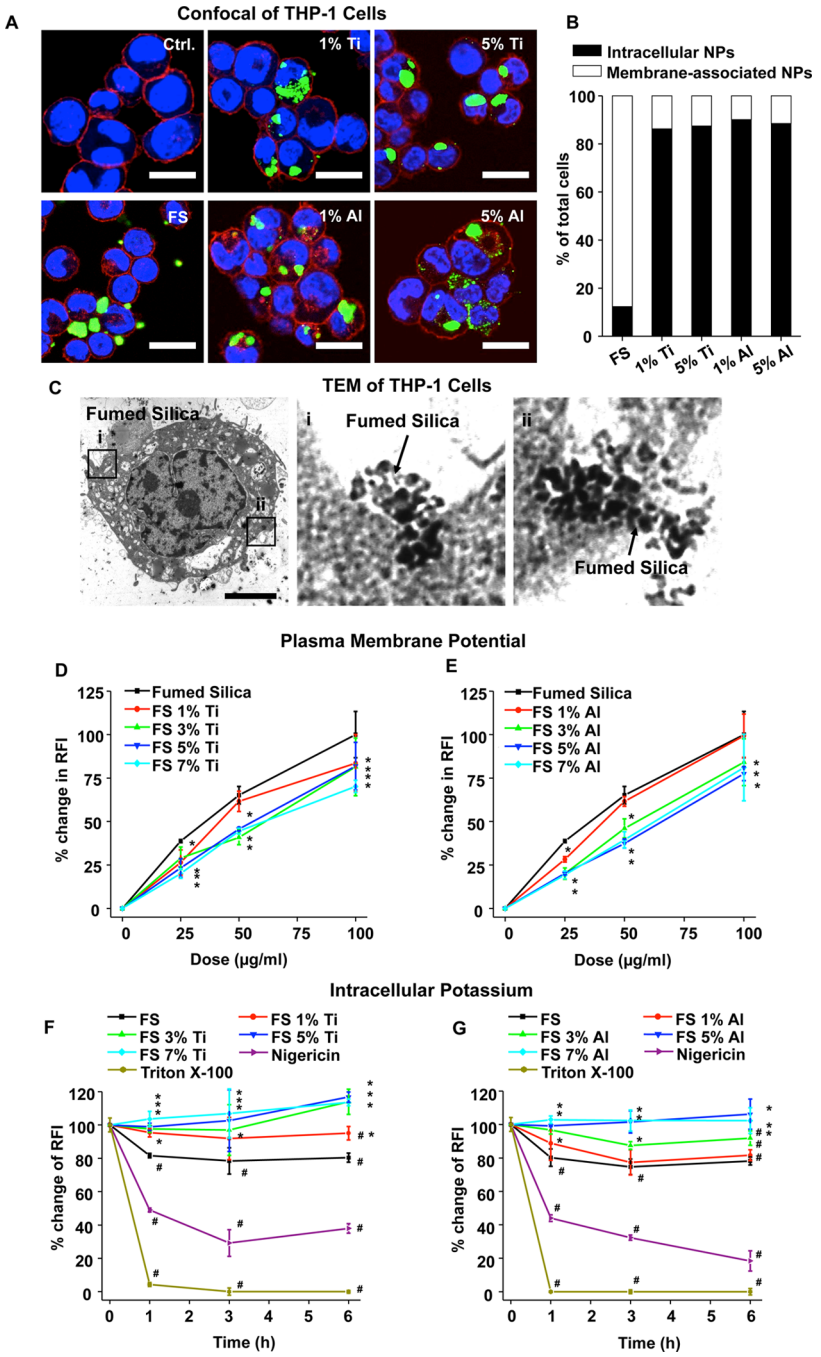

Figure 6. Fumed silica-induced plasma membrane perturbation and potassium efflux were attenuated by doping. (A) Confocal images of THP-1 cells treated with FITC-labeled nondoped and doped fumed nanoparticles. PMA-differentiated THP-1 cells were exposed to fumed silica (100 μg/mL) for 12 h in the presence of LPS (10 ng/mL). The scale bar is 20 μm. The cell membrane was stained red with Alexa Fluor 594 WGA; fumed silica was tagged with a green fluorescent marker (FITC), and the nucleus was stained with Hoechst 33342 (blue). (B) Percent of cells with either membrane-associated or intracellular particles was determined by counting ~100 cells per group. (C) TEM analysis of nondoped fumed-silica-treated THP-1 cells. PMA-differentiated THP-1 cells were exposed to fumed silica (100 μg/mL) for 12 h in the presence of LPS (10 ng/mL). The images were taken with a JEOL 100CX electron microscope at 80 kV. The scale bar is 5 μm. (D,E) Assessment of surface membrane depolarization by fumed silica using the FLIPR assay. THP-1 cells were incubated with 25−100 μg/mL of (D) Ti-doped and (E) Al-doped fumed silica nanoparticles in the presence of LPS (10 ng/mL). Nondoped fumed silica served as the control. Data were expressed as relative fluorescence intensity (RFI), the fluorescence intensity of particle-treated cells divided by that of control cells; *$p < 0.05$ compared to nondoped fumed-silica-treated cells. (F,G) Potassium efflux by fumed silica in THP-1 cells. Kinetic change of the cellular potassium levels as a result of potassium efflux during exposure to 100 μg/mL of (F) Ti-doped and (G) Al-doped fumed silica, in the presence of LPS (10 ng/mL). THP-1 cells, exposed to fumed silica, were stained with 5 μM PBFI-AM for 1 h. Nigericin (15 μM) and Triton X-100 (0.2%) were used as positive controls. Data were expressed as RFI, which is defined as the fluorescence intensity of particle-treated cells normalized to the intensity of control cells; *$p < 0.05$ compared to nondoped fumed-silica-treated cells; $^{\#}p < 0.05$ compared to control cells.

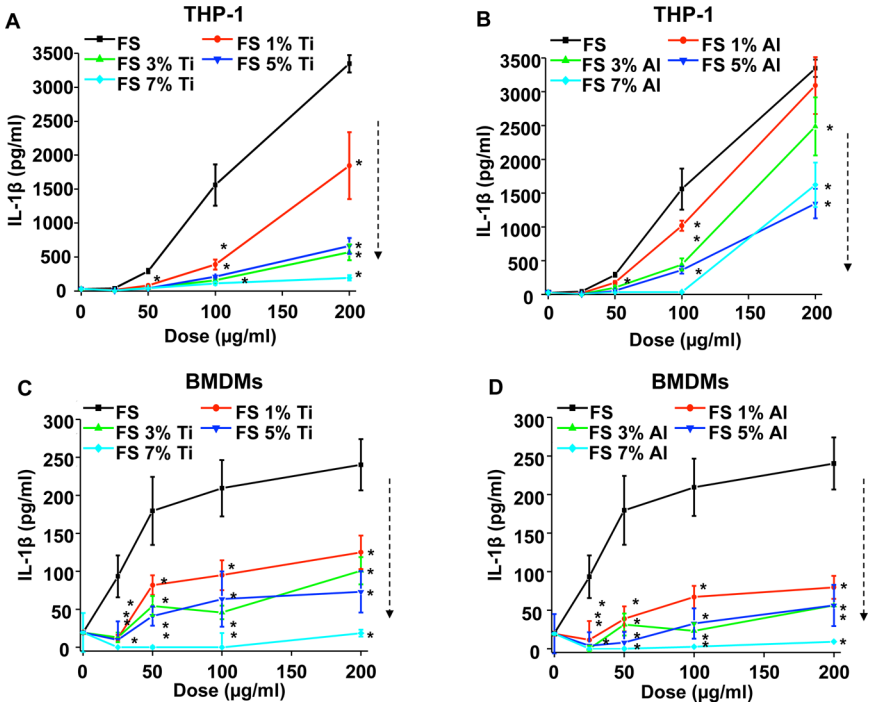

Figure 7. Reduction in IL-1β production by Ti and Al doping of fumed silica nanoparticles. (A,B) IL-1β production induced by doped fumed silica in THP-1 cells. Naive THP-1 cells were treated with PMA (1 μg/mL) for 16 h. PMA-differentiated THP-1 cells were then exposed to 25−200 μg/mL of (A) Ti-doped and (B) Al-doped fumed silica nanoparticles for 24 h in the presence of LPS (10 ng/mL). IL-1β production was quantified by ELISA; *$p < 0.05$ compared to nondoped fumed silica. (C,D) IL-1β production induced by doped fumed silica in bone marrow-derived macrophages (BMDMs). BMDMs obtained from wild-type C57BL/6 mice were exposed to 25−200 μg/mL of (C) Ti-doped and (D) Al-doped fumed silica nanoparticles for 24 h in the presence of LPS (500 ng/mL); *$p < 0.05$ compared to nondoped fumed silica.

imaging plate reader (FLIPR).[37] This dye localizes in the lipid membrane and changes fluorescence intensity during collapse of the cellular ionic gradient. We found that pristine fumed silica could significantly depolarize the membrane at a dose of 25 μg/mL ($p < 0.05$) (Figure 6D,E); this is much lower than the dose required for cytotoxicity (≥100 μg/mL) (Figure S7). In comparison, Ti- or Al-doped particles had an incrementally reduced effect on membrane potential according to the doping level (Figure 6D,E).

Because the change in membrane potential can also be accompanied by changes in ionic flux (*e.g.*, Ca^{2+}, K^+, and Na^+) across the cell membrane, we chose K^+ as a representative ion to determine whether fumed silica impacts membrane flux in THP-1 cells by using a K^+-sensitive fluorophore, PBFI-AM.[38] This demonstrated that pristine fumed silica could induce a modest but significant ($p < 0.05$) K^+ efflux during a 6 h exposure. Triton X-100 (a surfactant) and Nigericin (a K^+ ionophore)[39] induced substantial potassium efflux (Figure 6F,G). In comparison, Ti or Al doping induced significantly less K^+ outflow ($p < 0.05$) (Figure 6F,G). In summary, we demonstrated that doping ameliorates the level of plasma membrane perturbation and collapse in ionic gradients (K^+ flux) induced by fumed silica nanoparticles.

Doping Attenuates Activation of the NLRP3 Inflammasome in Response to Membrane Perturbation and Generation of Cellular Oxidative Stress. The triggering of potassium efflux[40] and ability of fumed silica nanoparticles to generate oxygen radicals could trigger additional cellular responses that can enhance the pro-inflammatory effects of these materials. In particular, the NLRP3 inflammasome has been linked to the induction of IL-β production by a variety of ENMs, which are capable of assembling the NLRP3, ASC, and caspase-1 subunits of the inflammasome in response to stimuli originating at the surface membrane or cellular lysosomes.[18,19] In order to compare nondoped and doped fumed silica nanoparticles for their ability to induce the NLRP3 inflammasome activation, PMA-differentiated THP-1 cells were used to determine IL-1β release in the supernatant.[5,18,36] LPS (10 ng/mL) was added to prime the cells for pro-IL-1β production, thereby allowing the study of IL-1β release by the assembled NLRP3 inflammasome. LPS alone induced minimal IL-1β production in control cells. While pristine fumed silica could induce a dose-dependent increase in IL-1β production, incremental Ti or Al doping was associated with a progressive decrease in cytokine production (Figure 7A,B). We also expressed the increase in IL-1β production according to surface area dose[41,42] (Figure S8A,B). This demonstrated that the ranking of IL-1β levels by doped and nondoped particles remains similar to the mass dose effects shown in Figure 7. We also normalized IL-1β production in THP-1 cells according to the % viable cells, as determined by the MTS assay

to show that there is no change in the relative abundance and ranking of IL-1β production (Figure S8E,F). The involvement of the NLRP3 inflammasome was confirmed by failure of NLRP3-deficient (defNLRP3) and ASC-deficient (defASC) THP-1 cells to release IL-1β upon fumed silica nanoparticle exposure (Figure S9A,B). We also confirmed the results in BMDMs obtained from C57BL/6 mice[43,44] (Figure 7C,D and Supporting Information Figure S7E,F and Figure S8C,D,G,H). To demonstrate that this effect was not due to the presence of dopants, we physically mixed the nondoped fumed silica with either TiO_2 (anatase, primary size of 12.6 nm,[32] Table S1) or Al_2O_3 (γ phase, primary size of 14.7 nm,[32] Table S1) nanoparticles at the same weight ratios as doped materials. Particle mixing did not significantly affect IL-1β production, suggesting that doping is necessary and effective for ameliorating the pro-inflammatory effects of fumed silica (Figure S10A,B).

The role of K^+ efflux in inflammasome activation was confirmed by introducing a high concentration of K^+ into the THP-1 culture medium; this led to a marked suppression of IL-1β release (Figure S11). Because the fumed silica nanoparticle surface can spontaneously generate hydroxyl radicals (Figures 5 and S5), we asked whether this is associated with cellular oxidative stress in THP-1 cells. We demonstrated that fumed silica could significantly reduce cellular GSH levels ($p < 0.05$), which was ameliorated by Ti or Al doping (Figure 8A,B). The involvement of oxidative stress was further confirmed by using the thiol antioxidant, *N*-acetyl-L-cysteine (NAC), to demonstrate reduced IL-1β production in response to fumed silica (Figure 8C,D). Collectively, these data suggest that surface membrane perturbation, K^+ efflux, and cellular ROS production dynamically contribute to NLRP3 inflammasome activation and IL-1β production in a pathway that differs from that of high aspect ratio materials (*e.g.*, carbon nanotubes, aluminum oxyhydroxide), and rare earth oxides.[18,20,25] The latter materials induce inflammasome activation by damaging the lysosomal membrane.[18,20,25] This notion was supported by lack of evidence of lysosomal damage and cathepsin B release during treatment with fumed silica (data not shown).

Doping Ameliorates Acute Pulmonary Inflammation in the Mouse Lung. To further demonstrate the potential safety of doped silica, the particles acquired by doping with 3 and 7% of Ti or Al were used for oropharyngeal aspiration to assess the effects on pulmonary inflammation (Figure 9). The *in vivo* dose for animal experimentation was derived from a human occupational exposure of 10.5 mg/m^3 in a silica manufacturing facility.[45] Assuming ventilation of 20 L/min in a healthy human subject[46] and a particle deposition fraction of 30%, the estimated monthly exposure (8 h/day, 5 days/week for 4 weeks) of an adult would be 604.8 mg. Using a human lung alveolar surface area of 102 m^2, this is equivalent to a deposition level of 5929.4 μg/m^2 (Table S2). Assuming the same surface area dose will generate a biological

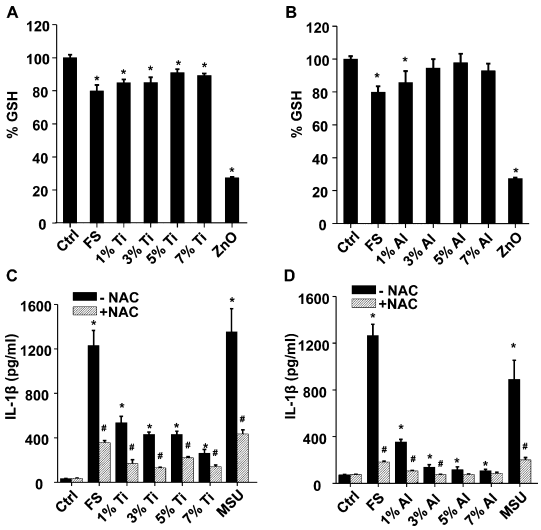

Figure 8. Reduction in cellular oxidative stress by Ti and Al doping of fumed silica nanoparticles. (A,B) Intracellular GSH levels in THP-1 cells after exposure to fumed silica. Naive THP-1 cells were treated with PMA (1 μg/mL) for 16 h. Then PMA-differentiated cells were exposed to 100 μg/mL of (A) Ti- and (B) Al-doped fumed silica for 6 h in the presence of LPS (10 ng/mL), and intracellular GSH level was determined using a GSH-Glo assay. Zinc oxide (50 μg/mL) was used as a positive control; *$p < 0.05$ compared to control. (C,D) NAC reduced the IL-1β production in THP-1 cells by fumed silica. THP-1 cells were pretreated with 25 μM of NAC for 30 min and then exposed to fumed silica (100 μg/mL) for 24 h in the presence of LPS (10 ng/mL). The IL-1β production was quantified by ELISA. Monosodium uric acid (50 μg/mL) was used as a positive control; $^{\#}p < 0.05$ compared to THP-1 cells of same particle treatment; *$p < 0.05$ compared to control cells without particle treatment.

equivalent response in mice as in humans, the equivalent surface area dose in a 25 g mouse equals 11.9 mg/kg, using an alveolar epithelial surface area of 0.05 m^2. This is equivalent to the 10 mg/kg dose used in our study. According to the Occupational Safety and Health Administration (OSHA), the threshold limit value (TLV) for amorphous silica is 80 mg/m^3, which translates to an exposure equivalent of 90 mg/kg in a mouse. Thus, our administered dose of 10 mg/kg falls within what is considered as a safe dose range by OSHA.

While doping with 7% Ti and Al led to a significant reduction of neutrophil influx ($p < 0.05$) into the BAL fluid compared to nondoped particles, 3% doping had lesser effects (Figure 9A). However, doping at 3 and 7% significantly reduced IL-1β release in the BAL fluid compared to nondoped particles ($p < 0.05$) (Figure 9B). We also tested a limited number of cytokines using single-antibody commercial ELISA kits, which demonstrated reduced MIP-1α and LIX (lipopolysaccharide-induced CXC chemokine) levels for 7% but not 3% doped particles, compared to pristine fumed silica (Figure 9C,D). The protective effect of doping was also confirmed by reduced focal inflammation in the lung, as demonstrated by hematoxylin and eosin (H&E) staining (Figure 9E). In summary, a modest level of doping was capable of reducing the acute

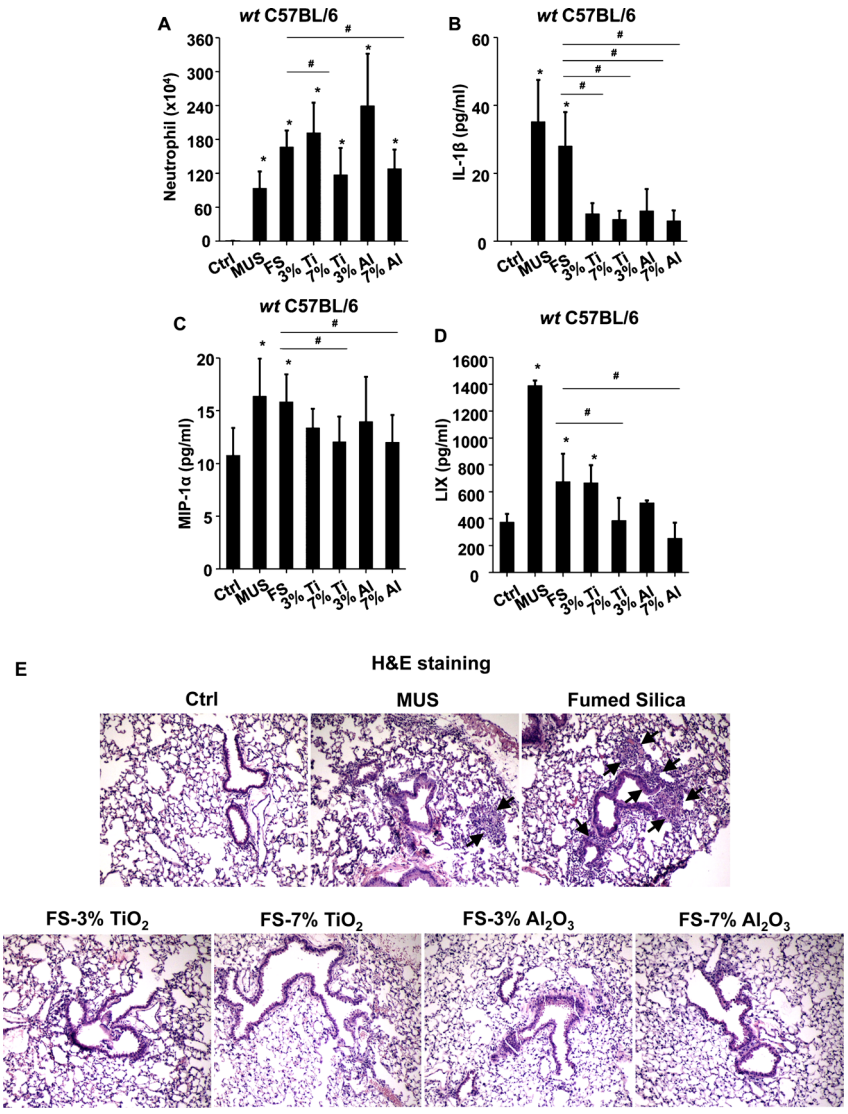

Figure 9. Ti and Al doping reduced pulmonary inflammation induced by fumed silica nanoparticles. C57BL/6 ($n = 6$) mice were exposed to 10 mg/kg of fumed silica by oropharyngeal aspiration. BAL fluid was collected to determine (A) neutrophil count, (B) IL-1β, (C) MIP-1α, and (D) LIX levels at 6 h. MIN-U-SIL, a natural form of crystalline silica, was used as a positive control; *$p < 0.05$ compared to control mice; #$p < 0.05$ compared to fumed-silica-treated mice. (E) H&E staining showed the presence of focal inflammation in the lungs, which was reduced by Ti and Al doping. The regions of focal inflammation are indicated by the arrows.

pro-inflammatory effects of fumed silica in the lung, suggesting that these materials could be used as a safer design procedure for use circumstances where exposure to fumed silica could lead to inhalation in the lung.

DISCUSSION

We demonstrated that a reduction of the density of reactive surface silanols on fumed silica leads to a reduction of the acute pro-inflammatory effects of these materials in the lung. While this effect could be achieved by calcination,[5] these silanols can easily be restored by experimental rehydration or during aging under moist atmospheric conditions. As an alternative approach to reducing silanol density, the replacement of Si with doped Ti or Al atoms results in permanent reduction in silanol display and a sustainable reduction in surface reactivity.[29,30] Additionally, since both Ti and Al and their oxide forms exhibit low toxicity,[30,31] doping should not lead to additional toxicity. We observed that Ti and Al doping yields fumed silica nanoparticles with a decreased potential for hydroxyl radical generation, less prone to perturb the plasma membrane or induce potassium efflux, NLRP3 inflammasome activation, and cytokine production in myeloid cells. This reduction of *in vitro* pro-inflammatory potential was accompanied by a reduction in acute inflammation in the murine lung, demonstrating that doping can serve as a safer design procedure for fumed silica.

The key finding of this study was that Ti or Al doping could reduce the toxicity of fumed silica nanoparticles through an impact on several toxicity mechanisms.

One doping effect is a decrease in the total number of silanol groups, as a result of the formation of titanol (Ti−OH) and aluminol (Al−OH) groups (Figure 4A,B and Supporting Information Figure S4A,B). The substitution of Si by Ti or Al at the fumed silica nanoparticle surface (Figure 4C) could disrupt hydrogen bonding between the neighboring hydroxyl groups, thus decreasing the spatial density of vicinal silanols, which are more reactive.[30] This notion is supported by Wang *et al.*, who reported that Al can have tetra-, penta-, and octa-coordination with surface silanol groups.[29] Penta-coordinated Al can result in hydrolysis shifting to form pseudobridged silanols that interact with the neighboring Al atoms.[47] This could disrupt the regular bonding of vicinal silanols by H-bonding, assuming there is a low percentage of germinal silanols ($=Si-(OH)_2$) in the total silanol pool.[48] A reduction of vicinal silanols could decrease the number of hydrogen donors that are available for complexing with quaternary/phosphate ester groups[12] or phospholipid trimethylammonium head groups. This will lead to a reduction in hemolysis or perturbation of the plasma membrane as key adverse outcome pathways in mediating fumed silica toxicity.[5,14,15]

In addition to lowering silanol display, doping also impacts the strained 3MR concentration and surface defects, which independently contribute to fumed silica toxicity.[5] Thermal quenching during the high-temperature fumed silica synthesis conditions results in the formation of strained 3MRs. We show that Ti progressively decreases the 3MR concentration with incremental doping levels (Figure S4D), possibly as a result of the displacement of Si with Ti atoms in some of the 3MRs. In addition to being able to reconstruct vicinal silanols, the 3MRs also participate in the formation of hydroxyl radicals through homolytic cleavage of siloxane bonds, which are reactive with water, oxygen, or hydrogen peroxide.[5,16,17] Doping may also reduce defect sites within the silica framework, as evidenced by our abiotic assays for ROS generation (Figures 5 and S5). These radical defects, which could include open bonds (E' centers, $\equiv Si\bullet$) or nonbridging oxygen hole centers,[49] are presumably produced in the high-temperature flame and are frozen within the silica framework by rapid cooling. The specific identification of the defect type as well as the mechanisms by which addition of Ti or Al precursors reduces defect concentration and the toxicity will require future studies of fumed silica formation and flame chemistry/physics.[50−52] Additionally, it is unknown if the changes in surface reactivity may lead to changes in the functionality of fumed silica when used in commercial products. For certain applications such as the anticaking effects of fumed silica in food, the changes may not be significant because calcination or doping does not change primary size, structure of the primary aggregate, surface area, or surface charge, which contributes to functionality.[53] Further research is needed to determine if the modifications could lead to changes in their functionality.

The use of doped materials also enhanced our understanding of a relatively novel surface membrane-mediated pathway leading to NLRP3 inflammasome activation, rather than originating from the cellular interior. The latter type of pathway is dependent on cellular uptake and lysosomal damage by rare earth oxides,[24] graphene,[54] and long aspect ratio materials (such as carbon nanotubes,[25] CeO_2,[36] AlOOH,[20] and Ag nanowires[44]). Lysosome damage leads to the release of cathepsin B, which acts as one of the stimuli for inflammasome activation. Instead, we show here that fumed silica interacts strongly with the plasma membrane, without significant cellular uptake (Figure 6A−C). The strength of the binding interaction of the fumed silica surface with the cell membrane leads to functional changes (Figure 6D,E), including K^+ efflux (Figure 6F, G), which is mechanistically linked to the NLRP3 inflammasome activation (Figure 7).[19,55,56] By reducing the surface silanol density as discussed above, doped fumed silica nanoparticles exhibit reduced membrane perturbation, potassium efflux, NLRP3 inflammasome activation, and cytotoxicity (Figures 6D−G and 7). These SARs also apply to the murine lung, where doping was associated with reduced lung inflammation (Figure 9). These relationships were also confirmed by using calcination and rehydration of the fumed particle as a less stable modification for showing this association (Figure 2).

As per Maynard's comment, care should be exercised in extrapolating research findings of material hazard to the likelihood that an engineered nanomaterial (such as fumed silica) will also lead to a toxicological outcome in humans during the real-life use conditions.[3] However, while fumed silica is generally considered safe for food applications, we show here that *in vitro* screening is predictive of potential lung injury by a bolus oropharyngeal exposure procedure, and that this warrants further study under aerosolized inhalation conditions, chronic exposures, and careful dose−response analysis. This type of dose response analysis should be developed based on real-life exposure scenario, such as in a manufacturing facility where exposure is expressed in a surface area dose that can be extrapolated to a related dose equivalent in an experimental animal, such as we demonstrate here. Our *in vivo* dose assessment also allows comparison to the OSHA TLV for fumed silica in an occupational environment. It would also be important to expand the *in vivo* analysis to include a range of commercial fumed silica nanoparticles, including materials that are used in the food industry as well as for chemical mechanical planarization in the semiconductor industry. Additionally, it would also be important to perform a comparative analysis of a library of fumed silica nanoparticles on their hazard potential in the lung *versus* the gastrointestinal (GI) tract. This could uncover

organ-specific differences, such as the bioavailability, transport, uptake, biopersistence, and clearance from the lung and GI tract. If, indeed, differences do exist, it would be important to know whether ingested fumed silica is rendered safe as a result of differences in the mucosal layer, mucus coating, digestive enzymes, heteroaggregation with food particles, pH, or other GI defense mechanisms. The GI tract presents a harsh environment in which pH variation from 1.5 to 8.5, hydrolytic enzymes, bile salts, mucus components, natural organic material, and the microbiome could play a significant role in rendering fumed silica less toxic. In contrast, when fumed silica is used in chili powder, paints, tires, and other products from which it could be aerosolized or inhaled, we may encounter a novel hazard that otherwise would not be considered under GRAS use conditions. It is possible that deposition of fumed silica nanoparticles deep in the lung at the level of the alveolar sac could provide access to the respiratory epithelium where the GRAS principle may not apply. Here, it may be appropriate to consider control measures and possibly safer design methodology.

CONCLUSIONS

In this study, we demonstrate that the acute inflammatory effects of fumed silica nanoparticles in the lung could be reduced by calcination or metal doping, both of which reduce surface expression of highly reactive silanols. While calcination provides a temporary solution, Ti and Al doping provides a stable reduction in surface reactivity and therefore a means of reducing the hazard potential of fumed silica. The mechanism of fumed-silica-induced toxicity involves membrane perturbation, potassium efflux, and NLRP3 inflammasome activation, all of which are addressed by the use of doped materials. Thus, Ti and Al doping could serve as safer alternative for commercial applications where there is inhalation risk.

EXPERIMENTAL SECTION

Reagents and Materials. Commercial fumed silica (AEROSIL, Evonik Degussa GmbH) was purchased from Sigma (St. Louis, MO); monosodium uric acid was purchased from InvivoGen (San Diego, CA); crystalline silica, MIN-U-SIL, 5 μm in size, was kindly provided by US SILICA (Berkeley Springs, WV); CA-074-Me was obtained from Sigma (St. Louis, MO); and NAC was purchased from American Regent, Inc. (Shirley, NY). The ELISA kits for human IL-1β and mouse LIX were purchased from R&D Systems (Minneapolis, MN), and the ELISA kit for mouse IL-1β was purchased from BD Biosciences (San Diego, CA).

Synthesis of Pure and Doped Fumed Silica Nanoparticles. Pure Ti- and Al-doped fumed silica nanoparticles were synthesized using flame spray pyrolysis. The required amounts of tetraethylorthosilicate (Si precursor, Sigma Adrich), aluminum secondary butoxide (Al precursor, Sigma Adrich), or titanium isopropoxide (Ti precursor, Sigma Adrich) were mixed together with xylene to provide 1−7% of Al and/or Ti by weight before combustion. As an example, for the 5% Ti- or Al-doped SiO_2 particles, 7.6 mL of 0.1 M Ti precursor (titanium isoproxide, Sigma-Aldrich) or 13.7 mL of 0.1 M Al precursor (aluminum secondary butoxide, Sigma-Aldrich) was mixed together with 50 mL of 0.5 M TEOS and sprayed in a single flame. During flame spray pyrolysis, the liquid precursors were delivered at a rate of 5 mL/min using a syringe pump and were atomized using 5 L/min O_2 at a constant pressure drop of 1.5 bar at the nozzle tip. The spray was ignited by a premixed co-delivery of CH_4 and O_2 (1.5 L/min, 3.2 L/min), forming a spray flame (Figure 1A). The ultrafine particles were formed by reaction, nucleation, surface growth, coagulation, and coalescence in the flame environment.[57] The particles were collected from a 257 mm glass filter placed in the flame reactor at the distance of 60 cm from the flame nozzle. For the calcination or rehydration process, fumed silica nanoparticles were heated in air to 800 °C for 6 h or after heating to 800 °C for 6 h followed by reflux in DI water for 24 h.

Characterization of Fumed Silica. FTIR spectra were recorded using a Bruker Vertex-70 FTIR spectrometer using the KBr pellet technique. High-throughput dynamic light scattering (HT-DLS, Dynapro Plate Reader, Wyatt Technology) was performed to determine the particle size and size distribution of the fumed silica nanoparticles in water, cell culture media, and PBS supplemented with BSA and DPPC following our recently developed protocol.[58] ζ-Potential measurement was conducted using a Brookhaven ZetaPALS instrument.

Dispersion of Fumed Silica in Exposure Media. Fumed silica was provided as dry powders. The samples were weighed in a fume hood on an analytical balance and suspended in deionized water at a concentration of 5 mg/mL. These suspensions were sonicated for 15 min in a water sonicator bath (Branson, Danbury, CT, model 2510, 100 W output power, 42 kHz frequency). An appropriate amount of fumed silica from each stock solution was added to the desired final concentration in cell culture media or PBS supplemented with BSA (0.6 mg/mL) and DPPC (0.01 mg/mL). The diluted particle suspensions were sonicated for 15 min to obtain well-dispersed particle suspensions at the desired final concentrations.

Determination of Fumed-Silica-Induced NLRP3 Inflammasome Activation and IL-1β Production. THP-1 cells in 100 μL of tissue culture media were plated at the density of 3×10^4 cells per well in a 96-well plate with addition of phorbol 12-myristate 13-acetate (PMA) (1 μg/mL) for 16 h. The medium was replaced, and the differentiated THP-1 cells were treated with fumed silica nanoparticles in the presence of LPS (10 ng/mL) for an additional 24 h. The supernatant of fumed-silica-exposed cells was collected for IL-1β assessment according to our previously developed protocol.[18] In another version of the experiment, THP-1 cells were pretreated with NAC (25 mM) for 30 min before the exposure of fumed silica nanoparticles. The medium was replenished, and the primed cells treated with fumed silica nanoparticles (100 μg/mL) in the presence of LPS (10 ng/mL) for 24 h. The supernatant of the stimulated cells was collected for IL-1β assessment. For primary BMDMs, cells in 100 μL of tissue culture media were plated at the density of 5×10^4 per well in a 96-well plate with the addition of LPS (500 ng/mL) for 5 h. The medium was replenished, and the primed cells were treated with fumed silica in the presence of LPS (10 ng/mL) for 24 h. The supernatant of the stimulated cells was collected for IL-1β assessment.

Evaluation of Intracellular Potassium Efflux. Fumed-silica-induced potassium efflux in THP-1 cells was determined using PBFI AM (Molecular Probes, Carlsbad, CA). Differentiated THP-1 cells were treated with fumed silica (100 μg/mL) in the presence of LPS for an indicated time. Then PBFI AM was added to the cells at the concentration of 5 μM, and cells were incubated at 37 °C and 5% CO_2 for 1 h. Nigericin (15 μM) and Triton X-100 (0.2%) treated cells were used as controls. The fluorescence of PBFI AM was measured at excitation/emission at 340/505 using a SpectraMax M5 microplate reader (Molecular Devices, Sunnyvale, CA).

Exposure of Fumed Silica Nanoparticles by Oropharyngeal Aspiration and Assessment of Exposure Outcomes. Eight week old male C57BL/6 mice were purchased from Charles River Laboratories (Hollister, CA). All animals were housed under standard laboratory conditions that have been set up according to UCLA guidelines for care and

treatment of laboratory animals as well as the NIH guide for the care and use of laboratory animals in research (DHEW78-23). These conditions are approved by the Chancellor's Animal Research Committee at UCLA and include standard operating procedures for animal housing (filter-topped cages; room temperature at 23 ± 2 °C; 60% relative humidity; 12 h light, 12 h dark cycle) and hygiene status (autoclaved food and acidified water). Animal exposure to fumed silica was carried out by an oropharyngeal aspiration method as described at NIOSH.[59] Briefly, animals were anesthetized by intraperitoneal injection of ketamine (100 mg/kg)/xylazine (10 mg/kg) in a total volume of 100 μL. With the anesthetized animals held in a vertical position, 50 μL of a PBS suspension, containing 40 μg of calcined or rehydrated commercial fumed silica, was instilled at the back of the tongue to allow pulmonary aspiration. In an experiment using doped fumed silica nanoparticles, an instillation dose of 250 μg was used. The mice were sacrificed 40 h later, upon which BAL fluid and lung tissues were collected as previously described.[60] Briefly, the trachea was cannulated, and the lungs were gently lavaged three times with 1 mL of sterile PBS to obtain BAL fluid. The BAL fluid was used for total and differential cell counting and for IL-1β, MIP-1α, and LIX measurements. Lung tissues were collected and stained with hematoxylin/eosin or with Masson's Trichrome staining. IL-1β and MIP-1α were measured by the ELISA kits. The ELISA microarray assay was performed as previous described.[61]

Statistical Analysis. All the experiments were repeated two to three times. For all the figures and tables, the values shown represent mean ± SD. Statistical significance was determined by two-tailed Student's *t* test for two-group analysis or one-way ANOVA for multiple group comparisons.

Conflict of Interest: The authors declare no competing financial interest.

Supporting Information Available: Additional details, figures, and tables as described in the text. The Supporting Information is available free of charge on the ACS Publications website at DOI: 10.1021/acsnano.5b03443.

Acknowledgment. This work was primarily supported by the U.S. Public Health Service Grant, R01 ES016746, with leveraged support from the National Science Foundation and the Environmental Protection Agency under Cooperative Agreement Number DBI 0830117 and 1266377. The authors thank Drs. Joel Pounds and Richard Zangar from Pacific Northwest National Laboratory for quantification of the cytokine production induced by calcinated/rehydrated fumed silica by an ELISA microarray assay. The authors thank the CNSI Advanced Light Microscopy/Spectroscopy Shared Facility at UCLA for confocal fluorescent microscopy, the use of TEM instruments at the Electron Imaging Center for NanoMachines supported by NIH (1S10RR23057 to Z.H.Z.), and CNSI at UCLA.

REFERENCES AND NOTES

1. Scribd, Inc. Fumed Silica Market; http://www.scribd.com/doc/37849468/Fumed-Silica-Market#scribd (accessed July 21, 2015).
2. Leung, C. C.; Yu, I. T. S.; Chen, W. Silicosis. *Lancet* **2012**, *379*, 2008–2018.
3. Maynard, A. D. Old Materials, New Challenges? *Nat. Nanotechnol.* **2014**, *9*, 658–659.
4. Sandberg, W.; Lag, M.; Holme, J.; Friede, B.; Gualtieri, M.; Kruszewski, M.; Schwarze, P.; Skuland, T.; Refsnes, M. Comparison of Non-Crystalline Silica Nanoparticles in IL-1beta Release from Macrophages. *Part. Fibre Toxicol.* **2012**, *9*, 32.
5. Zhang, H.; Dunphy, D. R.; Jiang, X.; Meng, H.; Sun, B.; Tarn, D.; Xue, M.; Wang, X.; Lin, S.; Ji, Z.; et al. Processing Pathway Dependence of Amorphous Silica Nanoparticle Toxicity: Colloidal vs Pyrolytic. *J. Am. Chem. Soc.* **2012**, *134*, 15790–15804.
6. Arts, J. H.; Muijser, H.; Duistermaat, E.; Junker, K.; Kuper, C. F. Five-Day Inhalation Toxicity Study of Three Types of Synthetic Amorphous Silicas in Wistar Rats and Post-Exposure Evaluations for up to 3 Months. *Food Chem. Toxicol.* **2007**, *45*, 1856–67.
7. Irfan, A.; Cauchi, M.; Edmands, W.; Gooderham, N. J.; Njuguna, J.; Zhu, H. Assessment of Temporal Dose-Toxicity Relationship of Fumed Silica Nanoparticle in Human Lung A549 Ccells by Conventional Cytotoxicity and (1)H-NMR-Based Extracellular Metabonomic Assays. *Toxicol. Sci.* **2014**, *138*, 354–64.
8. Gerloff, K.; Albrecht, C.; Boots, A. W.; Förster, I.; Schins, R. P. F. Cytotoxicity and Oxidative DNA Damage by Nanoparticles in Human Intestinal Caco-2 Cells. *Nanotoxicology* **2009**, *3*, 355–364.
9. van der Zande, M.; Vandebriel, R.; Groot, M.; Kramer, E.; Herrera Rivera, Z.; Rasmussen, K.; Ossenkoppele, J.; Tromp, P.; Gremmer, E.; Peters, R.; et al. Sub-Chronic Toxicity Study in Rats Orally Exposed to Nanostructured Silica. *Part. Fibre Toxicol.* **2014**, *11*, 8.
10. Nel, A.; Xia, T.; Meng, H.; Wang, X.; Lin, S.; Ji, Z.; Zhang, H. Nanomaterial Toxicity Testing in the 21st Century: Use of a Predictive Toxicological Approach and High-Throughput Screening. *Acc. Chem. Res.* **2013**, *46*, 607–621.
11. Sun, B.; Li, R.; Wang, X.; Xia, T. Predictive Toxicological Paradigm and High Throughput Approach for Toxicity Screening of Engineered Nanomaterials. *Int. J. Biomed. Nanosci. Nanotechnol.* **2013**, *3*, 4–18.
12. Nash, T.; Allison, A. C.; Harington, J. S. Physico-Chemical Properties of Silica in Relation to its Toxicity. *Nature* **1966**, *210*, 259–261.
13. Marks, J. The Neutralization of Silica Toxicity in vitro. *Occup. Environ. Med.* **1957**, *14*, 81–4.
14. Slowing, I. I.; Wu, C.-W.; Vivero-Escoto, J. L.; Lin, V. S. Y. Mesoporous Silica Nanoparticles for Reducing Hemolytic Activity Towards Mammalian Red Blood Cells. *Small* **2009**, *5*, 57–62.
15. Lin, Y.-S.; Haynes, C. L. Impacts of Mesoporous Silica Nanoparticle Size, Pore Ordering, and Pore Integrity on Hemolytic Activity. *J. Am. Chem. Soc.* **2010**, *132*, 4834–4842.
16. Sato, Y.; Kamo, S.; Takahashi, T.; Suzuki, Y. Mechanism of Free Radical-Induced Hemolysis of Human Erythrocytes: Hemolysis by Water-Soluble Radical Initiator. *Biochemistry* **1995**, *34*, 8940–8949.
17. Marar, T. Amelioration of Glucose Induced Hemolysis of Human Erythrocytes by Vitamin E. *Chem.-Biol. Interact.* **2011**, *193*, 149–53.
18. Wang, X.; Xia, T.; Duch, M.; Ji, Z.; Zhang, H.; Li, R.; Sun, B.; Lin, S.; Meng, H.; Liao, Y.-P.; et al. Pluronic F108 Coating Decreases the Lung Fibrosis Potential of Multiwall Carbon Nanotubes by Reducing Lysosomal Injury. *Nano Lett.* **2012**, *12*, 3050–3061.
19. Sun, B.; Wang, X.; Ji, Z.; Li, R.; Xia, T. NLRP3 Inflammasome Activation Induced by Engineered Nanomaterials. *Small* **2013**, *9*, 1595–1607.
20. Sun, B.; Ji, Z.; Liao, Y.-P.; Wang, M.; Wang, X.; Dong, J.; Chang, C. H.; Li, R.; Zhang, H.; Nel, A. E.; et al. Engineering an Effective Immune Adjuvant by Designed Control of Shape and Crystallinity of Aluminum Oxyhydroxide Nanoparticles. *ACS Nano* **2013**, *7*, 10834–10849.
21. Xia, T.; Zhao, Y.; Sager, T.; George, S.; Pokhrel, S.; Li, N.; Schoenfeld, D.; Meng, H.; Lin, S.; Wang, X.; et al. Decreased Dissolution of ZnO by Iron Doping Yields Nanoparticles with Reduced Toxicity in the Rodent Lung and Zebrafish Embryos. *ACS Nano* **2011**, *5*, 1223–35.
22. Zhang, H.; Pokhrel, S.; Ji, Z.; Meng, H.; Wang, X.; Lin, S.; Chang, C. H.; Li, L.; Li, R.; Sun, B.; et al. PdO Doping Tunes Band-Gap Energy Levels as Well as Oxidative Stress Responses to a Co3O4 p-Type Semiconductor in Cells and the Lung. *J. Am. Chem. Soc.* **2014**, *136*, 6406–6420.
23. George, S.; Pokhrel, S.; Ji, Z.; Henderson, B. L.; Xia, T.; Li, L.; Zink, J. I.; Nel, A. E.; Mädler, L. Role of Fe Doping in Tuning the Band Gap of TiO2 for the Photo-Oxidation-Induced Cytotoxicity Paradigm. *J. Am. Chem. Soc.* **2011**, *133*, 11270–11278.
24. Li, R.; Ji, Z.; Chang, C. H.; Dunphy, D. R.; Cai, X.; Meng, H.; Zhang, H.; Sun, B.; Wang, X.; Dong, J.; et al. Surface Interactions with Compartmentalized Cellular Phosphates Explain Rare Earth Oxide Nanoparticle Hazard and Provide

Opportunities for Safer Design. *ACS Nano* **2014**, *8*, 1771–1783.
25. Li, R.; Wang, X.; Ji, Z.; Sun, B.; Zhang, H.; Chang, C. H.; Lin, S.; Meng, H.; Liao, Y.-P.; Wang, M.; et al. Surface Charge and Cellular Processing of Covalently Functionalized Multiwall Carbon Nanotubes Determine Pulmonary Toxicity. *ACS Nano* **2013**, *7*, 2352–2368.
26. Xia, T.; Kovochich, M.; Liong, M.; Zink, J. I.; Nel, A. E. Cationic Polystyrene Nanosphere Toxicity Depends on Cell-Specific Endocytic and Mitochondrial Injury Pathways. *ACS Nano* **2008**, *2*, 85–96.
27. Joshi, S.; Ghosh, I.; Pokhrel, S.; Mädler, L.; Nau, W. M. Interactions of Amino Acids and Polypeptides with Metal Oxide Nanoparticles Probed by Fluorescent Indicator Adsorption and Displacement. *ACS Nano* **2012**, *6*, 5668–5679.
28. Pokhrel, S.; Nel, A. E.; Mädler, L. Custom-Designed Nanomaterial Libraries for Testing Metal Oxide Toxicity. *Acc. Chem. Res.* **2013**, *46*, 632–641.
29. Wang, Z.; Pokhrel, S.; Chen, M.; Hunger, M.; Mädler, L.; Huang, J. Palladium-Doped Silica−Alumina Catalysts Obtained from Double-Flame FSP for Chemoselective Hydrogenation of the Model Aromatic Ketone Acetophenone. *J. Catal.* **2013**, *302*, 10–19.
30. Huang, J.; van Vegten, N.; Jiang, Y.; Hunger, M.; Baiker, A. Increasing the Brønsted Acidity of Flame-Derived Silica/Alumina up to Zeolitic Strength. *Angew. Chem., Int. Ed.* **2010**, *49*, 7776–7781.
31. Xia, T.; Kovochich, M.; Liong, M.; Mädler, L.; Gilbert, B.; Shi, H.; Yeh, J. I.; Zink, J. I.; Nel, A. E. Comparison of the Mechanism of Toxicity of Zinc Oxide and Cerium Oxide Nanoparticles Based on Dissolution and Oxidative Stress Properties. *ACS Nano* **2008**, *2*, 2121–2134.
32. Zhang, H.; Ji, Z.; Xia, T.; Meng, H.; Low-Kam, C.; Liu, R.; Pokhrel, S.; Lin, S.; Wang, X.; Liao, Y.-P.; et al. Use of Metal Oxide Nanoparticle Band Gap To Develop a Predictive Paradigm for Oxidative Stress and Acute Pulmonary Inflammation. *ACS Nano* **2012**, *6*, 4349–4368.
33. Nel, A. E.; Mädler, L.; Velegol, D.; Xia, T.; Hoek, E. M. V.; Somasundaran, P.; Klaessig, F.; Castranova, V.; Thompson, M. Understanding Biophysicochemical Interactions at the Nano-Bio Interface. *Nat. Mater.* **2009**, *8*, 543–557.
34. Matsuda, A.; Kogure, T.; Matsuno, Y.; Katayama, S.; Tsuno, T.; Tohge, N.; Minami, T. Structural-Changes of Sol Gel-Derived TIO2-SIO2 Coatings in an Environment of High-Temperature and High Humidity. *J. Am. Ceram. Soc.* **1993**, *76*, 2899–2903.
35. Voigt, A.; Murugavel, R.; Ritter, U.; Roesky, H. W. Infrared and Si-29 NMR Spectroscopic Investigations on Metallasiloxanes Derived from Organosilanetriols. *J. Organomet. Chem.* **1996**, *521*, 279–286.
36. Ji, Z.; Wang, X.; Zhang, H.; Lin, S.; Meng, H.; Sun, B.; George, S.; Xia, T.; Nel, A.; Zink, J. Designed Synthesis of CeO_2 Nanorods and Nanowires for Studying Toxicological Effects of High Aspect Ratio Nanomaterials. *ACS Nano* **2012**, *6*, 5366–5380.
37. Zhang, H.; Xia, T.; Meng, H.; Xue, M.; George, S.; Ji, Z.; Wang, X.; Liu, R.; Wang, M.; France, B.; et al. Differential Expression of Syndecan-1 Mediates Cationic Nanoparticle Toxicity in Undifferentiated versus Differentiated Normal Human Bronchial Epithelial Cells. *ACS Nano* **2011**, *5*, 2756–2769.
38. Bortner, C. D.; Cidlowski, J. A. Caspase Independent/Dependent Regulation of K+, Cell Shrinkage, and Mitochondrial Membrane Potential during Lymphocyte Apoptosis. *J. Biol. Chem.* **1999**, *274*, 21953–21962.
39. Al-Mehdi, A. B.; Ischiropoulos, H.; Fisher, A. B. Endothelial Cell Oxidant Generation during K(+)-Induced Membrane Depolarization. *J. Cell. Physiol.* **1996**, *166*, 274–280.
40. Petrilli, V.; Papin, S.; Dostert, C.; Mayor, A.; Martinon, F.; Tschopp, J. Activation of the NALP3 Inflammasome is Triggered by Low Intracellular Potassium Concentration. *Cell Death Differ.* **2007**, *14*, 1583–1589.
41. Oberdorster, G.; Oberdorster, E.; Oberdorster, J. Nanotoxicology: an emerging discipline evolving from studies of ultrafine particles. *Environ. Health Perspect.* **2005**, *113*, 823–39.
42. Taylor, U.; Rehbock, C.; Streich, C.; Rath, D.; Barcikowski, S. Rational design of gold nanoparticle toxicology assays: a question of exposure scenario, dose and experimental setup. *Nanomedicine* **2014**, *9*, 1971–1989.
43. Lin, S.; Wang, X.; Ji, Z.; Chang, C. H.; Dong, Y.; Meng, H.; Liao, Y.-P.; Wang, M.; Song, T.-B.; Kohan, S.; et al. Aspect Ratio Plays a Role in the Hazard Potential of CeO2 Nanoparticles in Mouse Lung and Zebrafish Gastrointestinal Tract. *ACS Nano* **2014**, *8*, 4450–4464.
44. Sun, B.; Wang, X.; Ji, Z.; Wang, M.; Liao, Y.-P.; Chang, C. H.; Li, R.; Zhang, H.; Nel, A. E.; Xia, T. NADPH Oxidase-Dependent NLRP3 Inflammasome Activation and its Important Role in Lung Fibrosis by Multiwalled Carbon Nanotubes. *Small* **2015**, *11*, 2087–97.
45. Choudat, D.; Frisch, C.; Barrat, G.; el Kholti, A.; Conso, F. Occupational Exposure to Amorphous Silica Dust and Pulmonary Function. *Occup. Environ. Med.* **1990**, *47*, 763–766.
46. Wang, X.; Ji, Z.; Chang, C. H.; Zhang, H.; Wang, M.; Liao, Y.-P.; Lin, S.; Meng, H.; Li, R.; Sun, B.; et al. Use of Coated Silver Nanoparticles to Understand the Relationship of Particle Dissolution and Bioavailability to Cell and Lung Toxicological Potential. *Small* **2014**, *10*, 385–398.
47. Chizallet, C.; Raybaud, P. Pseudo-Bridging Silanols as Versatile Brønsted Acid Sites of Amorphous Aluminosilicate Surfaces. *Angew. Chem., Int. Ed.* **2009**, *48*, 2891–2893.
48. March, H. N.; Mucci, J. F. *Chemical Physics of Free Molecules*; Springer: Berlin, 1993.
49. Sahl, R. Defect Related Luminescence in Silicon Dioxide Netowrk: A Review. In *Crystalline Silicon—Properties and Uses*; Basu, S., Ed.; InTech: Rijeka, Croatia, 2011; pp 135−172.
50. Khavryuchenko, V. D.; Khavryuchenko, O. V.; Lisnyak, V. V. Formation of Pyrogenic Silica: Spectroscopic and Quantum Chemical Insight. *Crit. Rev. Solid State Mater. Sci.* **2011**, *36*, 47–65.
51. Moore, T.; Brady, B.; Martin, L. R. Measurements and Modeling of SiCl4 Combustion in a Low-Pressure H2/O2 Flame. *Combust. Flame* **2006**, *146*, 407–418.
52. Shekar, S.; Sander, M.; Riehl, R. C.; Smith, A. J.; Braumann, A.; Kraft, M. Modelling the Flame Synthesis of Silica Nanoparticles from Tetraethoxysilane. *Chem. Eng. Sci.* **2012**, *70*, 54–66.
53. Wagner, N. J.; Brady, J. F. Shear thickening in colloidal dispersions. *Phys. Today* **2009**, *62*, 27–32.
54. Wang, X.; Duch, M. C.; Mansukhani, N.; Ji, Z.; Liao, Y.-P.; Wang, M.; Zhang, H.; Sun, B.; Chang, C. H.; Li, R.; et al. Use of a Pro-Fibrogenic Mechanism-Based Predictive Toxicological Approach for Tiered Testing and Decision Analysis of Carbonaceous Nanomaterials. *ACS Nano* **2015**, *9*, 3032–3043.
55. Franchi, L.; Kanneganti, T. D.; Dubyak, G. R.; Nunez, G. Differential Requirement of P2 × 7 Receptor and Intracellular K+ for Caspase-1 Activation Induced by Intracellular and Extracellular Bacteria. *J. Biol. Chem.* **2007**, *282*, 18810–8.
56. Munoz-Planillo, R.; Kuffa, P.; Martinez-Colon, G.; Smith, B. L.; Rajendiran, T. M.; Nunez, G. K(+) Efflux is the Common Trigger of NLRP3 Inflammasome Activation by Bacterial Toxins and Particulate Matter. *Immunity* **2013**, *38*, 1142–53.
57. Pokhrel, S.; Birkenstock, J.; Schowalter, M.; Rosenauer, A.; Mädler, L. Growth of Ultrafine Single Crystalline WO3 Nanoparticles Using Flame Spray Pyrolysis. *Cryst. Growth Des.* **2010**, *10*, 632–639.
58. Ji, Z.; Jin, X.; George, S.; Xia, T.; Meng, H.; Wang, X.; Suarez, E.; Zhang, H.; Hoek, E. M. V.; Godwin, H.; et al. Dispersion and Stability Optimization of TiO2 Nanoparticles in Cell Culture Media. *Environ. Sci. Technol.* **2010**, *44*, 7309–7314.
59. Shvedova, A. A.; Kisin, E.; Murray, A. R.; Johnson, V. J.; Gorelik, O.; Arepalli, S.; Hubbs, A. F.; Mercer, R. R.; Keohavong, P.; Sussman, N.; et al. Inhalation vs. Aspiration of Single-Walled Carbon Nanotubes in C57BL/6 Mice: Inflammation, Fibrosis, Oxidative Stress, and Mutagenesis. *Am. J. Physiol.: Lung Cell. Mol. Physiol.* **2008**, *295*, L552–L565.

60. Hao, M.; Comier, S.; Wang, M.; Lee, J. J.; Nel, A. Diesel Exhaust Particles Exert Acute Effects on Airway Inflammation and Function in Murine Allergen Provocation Models. *J. Allergy Clin. Immunol.* **2003**, *112*, 905–914.
61. Servoss, S. L.; Gonzalez, R.; Varnum, S.; Zangar, R. C. High-Throughput Analysis of Serum Antigens using Sandwich ELISAs on Microarrays. *Methods Mol. Biol.* **2009**, *520*, 143–50.